



**Post-plasma catalysis: Charge effect on product selectivity
in conversion of methane and nitrogen plasma to ethylene
and ammonia**

Journal:	<i>Catalysis Science & Technology</i>
Manuscript ID	CY-ART-12-2022-002077.R1
Article Type:	Paper
Date Submitted by the Author:	01-Mar-2023
Complete List of Authors:	Tiwari, Sarojini; West Virginia University, Chemical Engineering Ibrahim, Saleh Ahmat; University of Massachusetts Lowell Downtown Bookstore - UMASS Lowell Downtown Robinson, Brandon; West Virginia University, Chemical Engineering Brown, Sean; West Virginia University, Chemical and Biomedical Engineering Wang, Qiang; West Virginia University Che, Fanglin; University of Massachusetts Lowell Downtown Bookstore - UMASS Lowell Downtown Hu, Jianli; West Virginia University, Chemical Engineering

Post-plasma catalysis: Charge effect on product selectivity in conversion of methane and nitrogen plasma to ethylene and ammonia

Sarojini Tiwari^{1†}, Saleh Ahmat Ibrahim^{2†}, Brandon Robinson¹, Sean Brown¹, Qiang Wang³, Fanglin Che^{2*}, Jianli Hu^{1*}

¹Department of Chemical and Biomedical engineering, West Virginia University, Morgantown, USA

²Department of Chemical Engineering, University of Massachusetts Lowell, Lowell, USA

³Material Characterization Facilities, West Virginia University, Morgantown, USA

Abstract: The main challenge in simultaneous conversion of methane and nitrogen to ethylene and ammonia under plasma conditions is the low selectivity. This is largely due to the difficulties in controlling the reactions among the plasma-excited reactive intermediates. To address this challenge, we explored an innovative strategy - post-plasma catalysis outside a microwave-enhanced plasma zone (MWP). Experimentally, the post-plasma species, such as CH_x , NH_x , CN , and C_2H_x , from a feed-gas mixture of methane, nitrogen and Argon were identified using an optical emission spectrometer. In the absence of a catalyst but under plasma condition, methane and nitrogen could only convert to hydrogen cyanide, acetylene, and hydrogen. After placing the thermally heated Ag-Pd/CeO₂ catalyst in the post plasma region, the selectivity of hydrogen cyanide was reduced by 9%, while the active nitrogen-based species simultaneously generated a steady amount of ammonia (selectivity=9%). The selectivity of ethylene increased from 3% to 37%, the highest among the C₂ products. While under conventional thermal heating, in absence of plasma, the same catalyst over-hydrogenated the acetylene to ethane and no ammonia was produced from nitrogen. Theoretically, density functional theory calculations (DFT) determined that the post-plasma species-induced positive charge over the Pd-Ag catalytic surface could enhance the energetics of forming ethylene but suppress the energetics of its further hydrogenation to ethane. Overall, this combined experimental and theoretical study advanced the fundamental understanding of the effects of post-plasma species on optimizing the selectivity in heterogeneous catalysis.

Keywords: Microwave plasma, post-plasma catalysis, methane conversion, plasma-catalyst hybrid reactor, density functional theory

† S. Tiwari, S. A. Ibrahim contributed equally.

*Corresponding authors emails: john.hu@mail.wvu.edu; fanglin_che@uml.edu

1. Introduction

Shale gas, one of the unconventional resources of natural gas, is projected to be the major contributor to carbon free economy around the globe [1]. The escalating extraction technology and government incentives have made shale gas inexpensive. However, the environmental challenges in its transportation to the current processing plants has limited its optimum utilization. One way to eliminate this obstruction is to cut down the transportation of natural gas to the processing plants and convert it to useful products at the production stage. This can only be achieved through the principles of process intensification [2].

Chemical processing industry is substantially dependent on natural gas as a feedstock. In the process, it has become one of the major contributors of green-house gas emissions [3]. Process intensification can substantially upgrade chemical industries to a carbon free and zero waste systems. The basic definition of an intensified chemical process has broadened from merely reducing the size of the processing plant to a holistic undertaking that can reduce waste and energy consumption with improved product yield [2][4]. The direct conversion of methane (CH_4), the major component in shale gas, to value-added chemicals can be qualified as an intensified process, if it is energy efficient, free of unwanted side products (CO_2), and leads to maximum conversion of CH_4 to useful products.

Microwave plasma (MWP) reactor is an emerging technology in line with the principles of process intensification. It offers several benefits such as fast process dynamics and flexibility, high product yield with least amount of unwanted by-products and low maintenance cost [5]. Additionally, MWP offers several advantages over other plasma sources [6]. It does not require electrodes, have the

highest electron density in the discharge region, and high power-to-plasma efficiency [7]. In fact, the direct conversion of CH₄ to acetylene (C₂H₂) and hydrogen (H₂) in MWP reactors have been demonstrated to be energy efficient with high yield of the desired product [8][9]. They can be optimized further by changing process parameters such as MW power and frequency [10], and composition of the feed gas mixture [11]. However, MWP, being a high energy discharge, converts CH₄ mostly to H₂, C₂H₂, and undesired carbon soot [12]. One strategy to improve the above selectivity issue is to place a catalyst away from the discharge cavity, which is termed as post-plasma catalysis. Catalytic reactions in hot plasmas, such as MWP at atmospheric pressure, is only feasible in a post-plasma setup. In this kind of reactor, some of the plasma species created in the discharge region survive up to the post-plasma region [13]. Several studies have identified post-plasma species, such as CH, CH₂, CN, NH, and NH₂, in MWP reactors generated from a feed gas mixture of CH₄ with argon (Ar) or with nitrogen (N₂), directed at surface coating and nitriding applications [14–16]. Hybrid plasma-catalytic reaction systems driven by electrode-based non-thermal plasma sources such as DC, AC and nano-pulsed discharges, have been reported to convert methane to ethylene in a single pass. High ethylene yield from methane using Ag-Pd-Y zeolite and Lindlar catalyst have been reported by Gordon et al. [17] and Kado et al. [18] respectively. Wang et al. [19] demonstrated high yield ethylene production from methane in a two-step AC plasma-catalytic reaction system. In a similar reactor, Wang and Guan considerably improved the ethylene yield using recycle streams within the hybrid reactor [20]. Taking a step forward in terms of energy consumption, Delikonstantis et al. [21] reported a low-cost, high-yield ethylene production from methane in a hybrid plasma-catalytic reactor powered by nano-pulsed discharge using Pd and Au based catalyst. The objective of these non-thermal plasma-catalytic reactor system have been to optimize the yield of ethylene while improving upon the energy cost. None have focused on the understanding the interaction of plasma species with the catalyst surface using a thermal plasma source such as Microwave plasma operated at atmospheric pressure, in a hybrid plasma-catalytic system. In the current work, we have investigated the interaction of post-plasma species from methane and nitrogen plasma and a preheated catalyst placed in a furnace in the post plasma region

and demonstrated their role in reducing the amount of unwanted product (hydrogen cyanide) and improving the selectivity of desired products (ethylene and ammonia).

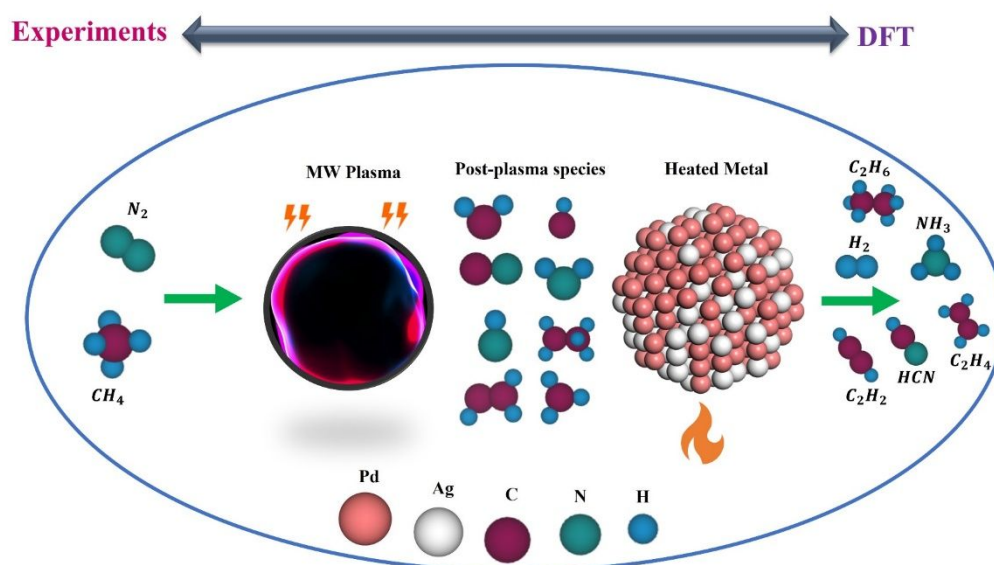


Figure 1: Reaction scheme for the post-plasma catalytic conversion of CH_4 and N_2

The influence of the plasma species on a catalyst can be established if the post-plasma species affect the distribution and selectivity of the final products [22]. An optimum catalyst design can maximize the inter-molecular interaction of the post-plasma species. Hence, MWP catalytic reactor adheres to the principle of process intensification [4]. The reactive species with a plasma consist of free electrons, ions, radicals, and excited states of gas molecules. An ideal catalyst would optimize the recombination of these species on its surface to modify the activity and the selectivity of the reaction [23] [13]. This principle is most useful in designing an in-plasma catalyst, used in non-thermal plasma, but has neither been fully understood nor applied under the post-plasma conditions. The CO conversion in a water-gas shift reaction were much improved on catalyst exposed to DBD plasma [24]. In another reaction, ammonia reforming of methane showed significant improvement due to plasma-catalyst interactions [25].

In case of MWP, it is not possible to place a catalyst within the electro-magnetic field at atmospheric pressure due to the high temperature in the discharge region. Based on numerous evidence of long-lived plasma species, a catalyst can be designed to influence the recombination of active radicals in the post-plasma region. The MWP made from CH_4 is known to be rich in CH_x and H radicals [26]. A desired catalyst, placed at the post plasma region, should be capable of hydrogenating these radicals to ethylene, while preventing over hydrogenation to ethane. Palladium (Pd) based catalyst is widely studied in acetylene hydrogenation [27]. The hydrogenation over Pd is known to occur through hydride formation resulting in the adsorption of active hydrogen species (subsurface hydrogen) on the catalyst surface. The re-adsorption of the subsurface hydrogen can easily over-hydrogenate ethylene to ethane reducing its selectivity [28]. Alloying Pd with another metal such as silver (Ag), has been shown to improve ethylene selectivity by suppressing the formation of subsurface hydrogen and hence preventing its over-hydrogenation to ethane [29][30]. Bimetallic Ag-Pd based catalyst has been shown, through several experiments, to be efficient in selective hydrogenation of acetylene to ethylene [31–33]. Additionally, the surface defects on ceria nanoparticle are known to improve metal activity in hydrogenation reactions and has served as the catalyst for ammonia synthesis [34–36]. Based on the above findings, we selected Ag-Pd/CeO₂ as our post-plasma catalyst.

In order to achieve the broader goal of direct utilization of shale gas to make C_2H_4 and NH_3 , the most valuable end products in chemical industry, through process intensification, a novel catalytic process, post-plasma catalysis, was investigated in this work. In a lab-scale proof of experiment, the article investigated the influence of post plasma species on product distribution and selectivity in a hybrid MWP catalytic reactor. The plasma was made of equal mixture (1% by volume, each) of CH_4 and N_2 balanced with Ar. The active species were identified at the post plasma region with the help of a non-intrusive optical emission spectrometer (OES). Based on this identification, a bimetallic catalyst made of Ag and Pd supported on Ceria (Ag-Pd/CeO₂) was placed in the post plasma region and heated in a furnace to a moderate temperature of 250°C. The reaction scheme is

shown in Figure 1. A detailed reaction mechanism was hypothesized to explain the change in reaction behavior and product distribution.

Furthermore, density functional theory (DFT) calculations were used to investigate the mechanism of methane dehydrogenation into C_1 or coupling into C_2 hydrocarbon species over the catalytic Ag-Pd surface in the absence and presence of post-plasma-induced positive charged surface effects. The energetics of the possible reaction steps for hydrocarbon production from methane were initially performed without positive charged surface effects. Based upon the energetics of the most favorable reaction paths, we then explored the role of surface positive charge effects on tuning the most favorable reaction paths and the selectivity of ethylene over ethane production during the post-plasma reaction. It is worth mentioning that the objective of the study was to elucidate the reaction mechanism of plasma species over the catalyst towards the formation of desired products, i.e., ethylene and ammonia. Therefore, diluted feedstock was used to better control plasma in laboratory microwave equipment. In industrial setting, microwave plasma concentration can be adjusted and controlled with active cooling and other means. The optimization of plasma feed concentration, productivity and yields of product, and energy consumption was beyond the scope of this study.

2. Materials and Methods

2.1 Catalyst synthesis and characterization

The metal salts, Palladium Nitrate Dihydrate (40% Pd basis) and Silver Nitrate (> 99%, titration) were purchased from Sigma Aldrich. The catalyst was prepared using incipient wetness impregnation method. The appropriate amount of Palladium (Pd) and Silver (Ag) salts were dissolved in deionized water to create a catalyst composition of 0.5% Pd and 0.5 % Ag metals by weight. Each salt solution was evenly dispersed over Cerium (IV) oxide (CeO_2), (nano powder, <50 nm particle size, Sigma Aldrich). The solid mixture was first dried for 12 hours at 110° C and then calcined at 550° C for 5 hours at a ramp rate of 10 °C/minute and atmospheric pressure. CeO_2 without any metal loading was also dried and calcined in the same way. Before every reaction, 0.5 g of catalyst was placed in a quartz tube

and heated in a furnace to a temperature of 250 °C under the flow of 50% H₂ at atmospheric pressure. The H₂ flow was maintained up to an hour before flushing it out of the tube with pure Ar.

The catalyst was characterized using Transmission Electron Microscope (JEOL JEM-2100, TEM) and X-ray Photoelectron Spectroscopy (Physical Electronics PHI VersaProbe XPS). The survey spectra from XPS analysis (Figure S-1, supporting information) were used to calculate the elemental composition on the catalyst surface. TEM images were used to calculate the particle size distribution of the metal loadings (Ag and Pd), provided in Figure S-2 of supporting information.

2.2 Experimental methods

The schematics of the three types of experiments conducted in this article are shown Figure 2. The first type of reaction was a plasma reaction without any catalyst as shown in Figure 2a.

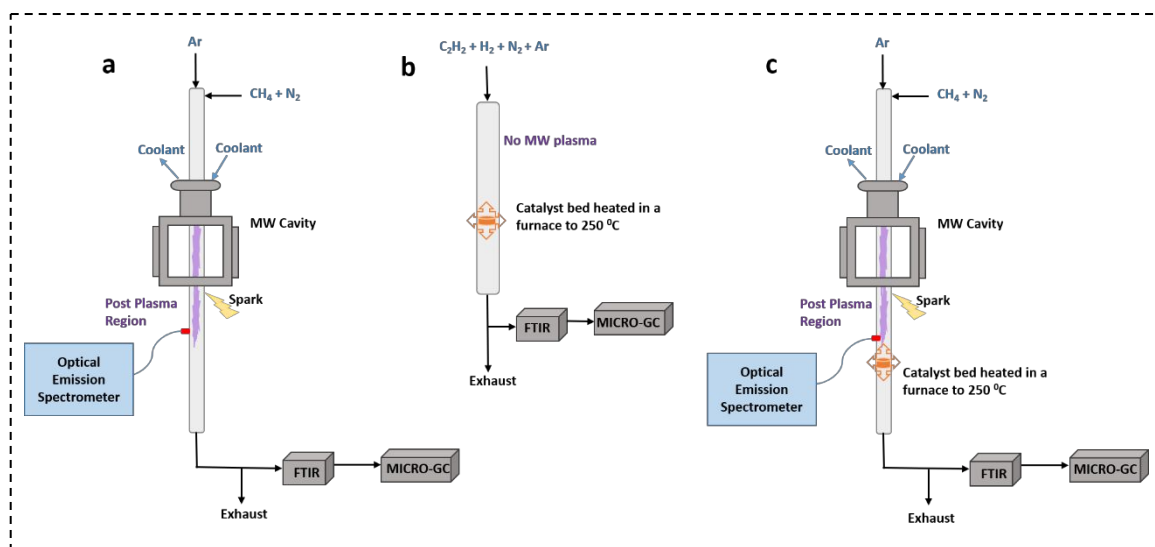


Figure 2: Schematics of the experiments (a) Plasma reaction, (b) Catalytic reaction without plasma, (c) Plasma reaction with a heated catalyst placed in the post-plasma region

The feed gas mixture consisted of 1% CH₄ and 1% N₂, by volume, balanced by Ar gas for a total inlet flow rate of 100 ml/min. The second reaction was carried out without plasma with a feed composition similar to the exit gas composition of the plasma reaction. The Ag-Pd/ Ceria catalyst was heated to 250

$^{\circ}\text{C}$ in a furnace and fed with a gas mixture of 1.5% H_2 , 1% N_2 , 0.25% C_2H_2 balanced with Ar (Figure 2b). In the third and final set of reactions, a catalyst (either Ag-Pd/Ceria or pretreated Ceria) was placed in the post plasma region and heated to 250 $^{\circ}\text{C}$ in a furnace. For the experimental proof-of-concept, concentration of methane and nitrogen was kept low to avoid temperature run-away in laboratory MWP reactor. In the industrial-scale settings, due to the presence of active cooling, higher concentration of methane and nitrogen can be used as the reactor feed.

At the beginning of every catalytic reaction, Ag-Pd/Ceria was first heated to 250 $^{\circ}\text{C}$ using a furnace (Mellen), equipped with a temperature controller in the post plasma region, as shown in Figure 2b and 2c in a gas flow mixture of 50% H_2 and 50% Ar. After an hour, hydrogen flow would be shut off and Ar would be allowed to flow through the reactor tube until all of hydrogen was flushed out. An optical emission spectrometer (OES) with a spectral range of 200-1100 nm, about 1 nm FWHM resolution and equipped with an optical fiber (Ocean Optics, HR2000_ES) was placed at the same location but only employed in plasma reactions with and without catalyst. Then, the microwave generator was put on at a set power of 450 W and an external spark was used to start the Ar plasma. The reactive gas mixture containing (CH_4 and N_2) would then be fed into the same quartz tube from a separate inlet point. The plasma would immediately change color from light blue (Ar plasma) to bright violet (CH_4 plasma). The typical purple color of N_2 plasma was not visible under the brightness of violet system emitted by the CH_4 plasma. The concentration of the product gas mixture was analyzed using Micro-GC (Agilent technologies, 3000, 2-channel) and FTIR-gas analyzer (600SC series, CAI) with DTGS detector type, spectral resolution of 0.8 cm^{-1} , and spectral range of 300-7500 cm^{-1} . The micro-GC and the FTIR-gas analyzer could analyze samples at the interval of 3 minutes and 1 minute, respectively. The microwave-enhanced plasma generation system consisted of a 2.45 GHz microwave generator, a sliding short-circuit tuner and a surface waveguide (Surfaguide, Sairem). The waveguide had an appropriate opening to insert a quartz tube (diameter= 0.25 inch, length= 50 cm) containing catalyst material. It was also provided with quick connectors for circulation of coolant (air). The picture of the experimental set-up is provided in Figure S-24 of supporting information. Every reaction was run for a duration of 20 minutes. Microwave enhanced-plasma is considered as thermal plasma when operated at atmospheric

pressure. The temperature in the discharge region can reach up to 1000 K [37]. Despite the air cooling, the discharge region was prone to reaching very high temperature due to ambient pressure conditions. The 20-minute run-time was found to be optimum to observe a steady production rate while preventing temperature run-away within the micro-wave discharge region.

The volume% of all the products were recorded directly at the FTIR and the micro-GC. The recorded values were then multiplied with the outlet total gas flow rate (102 sccm, monitored using a mass flow controller) and the resultant concentration profiles were plotted in Figure S-3 and S-4 of supporting information. The absolute selectivity of a given product 'i' was calculated using equation 1:

$$S_{ab,i} = \frac{C_i}{C_T} \times 100 \quad (1)$$

where, $S_{ab,i}$ was the absolute selectivity of product 'i', C_i was the exit concentration of the product 'i', C_T was the sum of exit concentration of all the products. The products $i = C_2H_4, C_2H_6, C_2H_2, NH_3, HCN,$ and H_2 .

The normalized selectivity of the C and N containing products were calculated using equation 2:

$$S_{N,j} = \frac{S_j}{S_T} \times 100 \quad (2)$$

where, $S_{N,j}$ was the normalized selectivity of the products 'j' : $C_2H_4, C_2H_6, C_2H_2, NH_3,$ and HCN . S_j was the selectivity of product 'j', and S_T was the sum of selectivity of all the products 'j'.

2.3 Computational methods

Density functional theory (DFT) calculations were performed using VASP (Vienna Ab-initio Simulation Package) software [38] [39]. Perdew-Burke-Ernzerhof (PBE) functionals and the projector-augmented wave (PAW) method were employed to describe the electron exchange-correlation and the ion-electron interactions, respectively [40–42]. The Monkhorst-Pack mesh of $(3 \times 3 \times 1)$ k-points and the plane-wave energy cutoff of 400 eV were applied to a four-layer $p(4 \times 4)$ Ag-Pd surface. Based on

experimental results, the molar ratio of Ag and Pd is 1:1 and they are perfectly mixed in the Ag-Pd catalyst. The bottom two layers of the catalytic surface were fixed to their bulk positions and the top two layers of the surface were relaxed to electronically interact with the adsorbates. The possible adsorption sites (Figure S-6, supporting information) of the Ag-Pd surface include top of Pd, top of Ag, bridge of Pd-Pd, bridge of Ag-Ag, bridge of Pd-Ag, fcc and hcp sites at the Pd-Ag interface [43]. The catalytic surface was tested using two different lattice constants, including the lattice constant of Ag of 4.159 Å and that of Pd of 3.953 Å, respectively. The calculated lattice constants of Ag and Pd are in agreement with both theoretical (4.136 Å and 3.890 Å) [44,45] and experimental (4.078 Å and 3.924 Å) [46,47] studies. The configurations were optimized when the electronic energy was converged to 10^{-5} eV and the ionic forces were smaller than 0.03 eV/Å.

Computational calculations were used to determine the adsorption configurations, adsorption energies and the reaction energies of all the intermediate species and elementary steps involved in hydrocarbon production from methane over the catalytic Ag-Pd surface. To investigate how post-plasma reactive species induced positively charged Ag-Pd surface will influence ethylene production over ethane production from reactant methane, we introduced the external positive electric field to polarize the surface to be positively charged. To simulate the positively charged catalytic surface in the supercell without adding or removing any charges, we applied the approach proposed by Neugebauer and Scheffler, where a dipole layer in the middle of vacuum with opposite charges at each side of the dipole layer was inserted [48,49]. Bader charge analysis was also applied in this study to understand the post-plasma species-induced positive charge effects on the post-plasma catalysis.

The most favorable energetics of the possible reaction pathways for hydrocarbon synthesis from methane over the Ag-Pd surface were first investigated without the positively charged surface effects (Figure 8a). Based on the adsorption configurations (Figures S-6 to S-19, supporting information), adsorption energies (Table S-2, supporting information), and reaction energies (Table S-3, supporting information) of the most favorable reaction pathways, we then applied the positively charged surface and optimized the adsorption/reaction during the hydrocarbon production process. The positive surface

charge (δ) was ranging from δ^0 0 to $\delta^{+0.6}$ with $\delta^{+0.1}$ increment being applied. The binding energy (E_{ad}) with and without positive charges (δ) can be calculated according to Eqn. (3):[38,43]

$$E_{ad} = E_{total} - E_{slab} - E_{adsorbate} \quad (3)$$

where E_{total} accounts for the total energy of the species over the surface with and without positive charges, E_{slab} corresponds to the energy of the surface with and without positive charge effects, and $E_{adsorbate}$ represents the energy of the adsorbate in the gas phase [43].

The adsorption energies of reaction-related intermediates as a function of the surface positive charges are shown in Figure S-21 and S-22, supporting information. Additionally, the reaction energy with the presence of the surface charges (δ) for the elementary reaction $A^* + B^* \rightarrow C^* + *$ is calculated as follows:

$$\Delta H_{rxn}(\delta) = E_{C^*}(\delta) + E_*(\delta) - E_{A^*}(\delta) - E_{B^*}(\delta) \quad (4)$$

Where $E_{A^*}(\delta)$, $E_{B^*}(\delta)$, $E_{C^*}(\delta)$ and $E_*(\delta)$ represent the total energies of species A^* , B^* , C^* and surface with surface charge effects, respectively.

The changes in adsorption energies or reaction energies raised by the positively charged surface are related to the dipole moments, polarizability, and the surface charges (Eqns. (5)-(6)) [45,47]. Theoretically, larger dipole moment and polarizability will possess larger surface charge effects on energetics [38].

$$E_{ad}(\delta) = E_{ad} - \vec{\mu} \cdot \delta - \frac{1}{2}\alpha|\delta|^2 \quad (5)$$

$$\Delta H_{rxn}(\delta) = \Delta H_{rxn} - \Delta\vec{\mu}_{rxn} \cdot \delta - \frac{1}{2}\Delta\alpha_{rxn}|\delta|^2 \quad (6)$$

Here, E_{ad} and ΔH_{rxn} correspond to the adsorption and reaction energies without surface charge effects, $\vec{\mu}$ and α represent the effective dipole moment and the polarizability for adsorbates adsorption over the surface. Moreover, $\Delta\vec{\mu}_{rxn}$ and $\Delta\alpha_{rxn}$ describe change in the effective dipole moment and polarizability

between products and reactants of the elementary reactions[40,43]. More theoretical details can be found in the supporting information.

3. Result and discussion

3.1 Identification of post-plasma species using Optical Emission Spectra (OES)

An optical emission spectrometer (OES) was employed to identify the post plasma species in our reaction system. The OES sensor was placed on the quartz tube around 20 cm away from the MW cavity during the plasma reactions. This distance was found to be appropriate to provide ample space for placing a furnace safely away from the microwave cavity while the OES could still pick up signals. The CN violet system (359.2 nm; 388.34 nm; 416.5 nm) and the C₂ swan system (473.7 nm; 516.52 nm) were the most dominant peaks observed on the spectra as shown in Figure 3 [50].

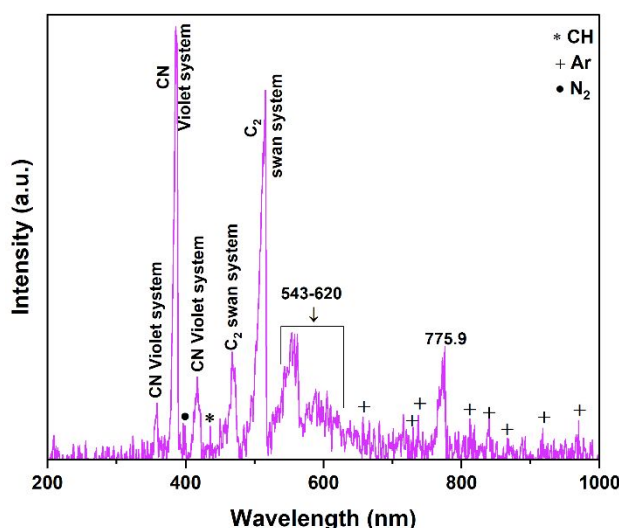


Figure 3: Optical emission spectra of the post-plasma region in a CH₄/N₂/Ar microwave plasma generated at 450 W, atmospheric pressure

Low intensity peaks of molecular N₂ (399.84 nm), CH (431 nm) and Ar were also detected [51] [52] [53]. Multiple overlapping peaks between 543-620 nm and at 775.9 nm could not be identified. The same peaks were also observed in the post plasma region of CH₄/Ar plasma. Since the Ar peaks are usually observed after 650 nm on OES spectra, these unidentified peaks may belong to CH or C₂ emissions.

3.2 Role of the post-plasma species in product formation

Atmospheric $\text{CH}_4/\text{N}_2/\text{Ar}$ plasmas are known to produce several active species and electrons leading to a complex plasma chemistry. There were three sets of reactions carried out to demonstrate the

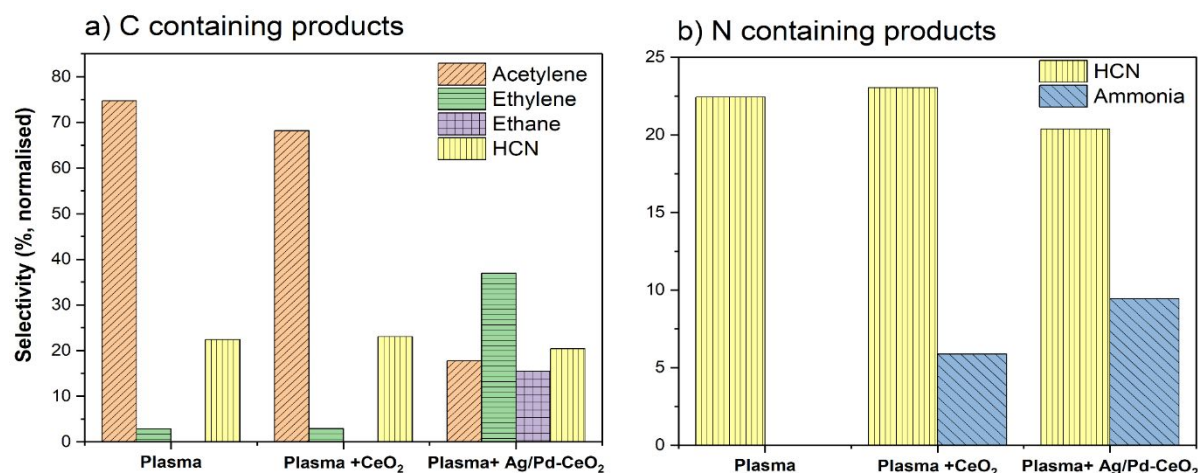


Figure 4: Normalized Selectivity of (a) C containing products, (b) N containing products for plasma only, plasma + CeO₂, and plasma + Ag-Pd/CeO₂ reactions

interaction between the post-plasma species and the catalyst. The first was a “plasma” reaction without any catalyst (Figure 2a). The second reaction was carried out with pretreated CeO₂ placed in the post plasma region and heated to 250 °C in a furnace, as shown in Figure 2c, designated as “plasma+ CeO₂”. In the third reaction, pretreated CeO₂ was replaced with Ag-Pd/CeO₂ in the post plasma region and similarly heated to 250°C in a furnace. This reaction was labelled as “Plasma+Ag-Pd/CeO₂”. The product distribution and normalized selectivity of carbon and nitrogen containing products in all three reactions, are shown in Figure 4. Note that hydrogen was the dominant product in all the reactions, hence it was omitted to avoid scaling issue.

As shown in Figure 4(a), acetylene had the highest selectivity of (~75%), followed by HCN with selectivity of 22% in plasma reaction. A small amount of ethylene was also produced with a selectivity of 3%. In plasma +CeO₂ reaction, the selectivity of acetylene, ethylene, and HCN were similar to the plasma reaction. In addition, ammonia was produced with a selectivity of almost 6% (Figure 4(b)). The product distribution changed considerably in the plasma + Ag-Pd/ CeO₂ reaction. The selectivity of both acetylene and HCN decreased to 18% and 20%, respectively. Ethylene had the highest selectivity of 37%. Ethane was also produced with a selectivity of around 16%, which is less than half of the

selectivity of ethylene. As shown in Figure 4 (b), the selectivity of ammonia increased slightly to around 9%. The production rate of all the products in ml/min are presented in Figure S-3 and S-4 of supporting information.

The plasma discharge within the MW cavity initiates the electron-molecule collisions leading to the activation of methane (CH_4) and nitrogen (N_2). Depending on the electron (e) energy, CH_4 can either rapidly dissociate into CH_x ($x=0,1,2,3$) and H radicals [54] or get ionized to disintegrate into charged CH_x^+ , C^+ and H species [55][56]. The peaks corresponding to H species (486.14 nm, 656.27 nm) are not visible on the OES spectra (Figure 3) due to the overlapping peaks of C_2 swan system. The excited N_2 molecules can ionize and dissociate to form species such as N_2^+ , N^+ and N within the discharge region [54][56]. The distinctive emission bands corresponding to N_2^+ at 358.21 nm and N^+ at 399.5 nm are not visible on the OES spectra (Figure 3) possibly due to the overlapping peaks of CN violet system. As explained later, the atomic N plays an important role in HCN formation and hence must be active in the post plasma region. The strong emissions of C_2 swan system indicates that the recombination of CH radicals continues in the post plasma region. This is confirmed by the presence of CH band on the OES spectra [52]. C_2H_4 may be produced by recombination of the CH_2 radicals. The collisions of atomic N with the CH_x radicals can produce HCN either directly or through the highly unstable H_2CN molecule [52,56]. It can also be formed through the direct reaction of CN with activated CH_4 species [57]. This is supported by the distinct CN emissions on the OES spectra collected from the post plasma region.

Ethane and ammonia were both absent in the product gas mixture of the plasma reactions without catalyst. The CH_3 radicals may have been rapidly consumed to form HCN before they could recombine to form ethane. The NH species which are the precursors to ammonia (NH_3) molecules, could have recombined to form N_2 and H_2 . A small amount of C_2H_4 was also observed during the plasma reaction without catalyst. Although majority of CH_2 radicals were consumed to form CN and HCN, some may have recombined to form C_2H_4 .

In case of plasma + CeO₂ and plasma + Ag-Pd/CeO₂, NH₃ gas was produced in addition to HCN, C₂H₂ and H₂ which is unlike the plasma reactions without catalyst (Figure S-4a). It is evident that the NH radicals were present in the post plasma region and were able to hydrogenate to NH₃ in presence of the moderately heated CeO₂ and Ag-Pd/CeO₂ [58]. The collision of CH₄ with ionized N₂ leads to the formation of NH radicals [52][59]. These radicals can also be formed by the combination of N and H species. The amount of ammonia gas produced were less than 20 ppm when the same post-plasma catalytic reaction was conducted on N₂/H₂/Ar plasma. Since this amount was ten times higher (~ 250 ppm) in case of CH₄/N₂/Ar plasma, it is highly probable that the CH₄ and N₂ collisions were the major source of NH radicals in our reaction system. The OES spectra band for NH radicals (336 nm) was not prominent in the post plasma region possibly due to its rapid consumption. The placement of heated CeO₂ in the post plasma region had no significant effect on the selectivity of HCN, acetylene and ethylene.

In case of plasma + Ag-Pd/Ce₂O reaction, the HCN selectivity was reduced. There was a considerable reduction in the selectivity of acetylene (Figure 4). Since all the CH radical recombination occurs in the post plasma region, it is evident that Ag-Pd/CeO₂ plays an important role in hydrogenating these radical to produce C₂H₄. The selective hydrogenation of acetylene (C₂H₂) on a typical bimetallic catalyst such as Ag-Pd/CeO₂ is believed to proceed via the adsorption of C₂H₂ on the catalyst surface. The chemisorbed acetylene (C₂H₂^{*}) is then converted to vinyl (CHCH₂^{*}) by dissociative adsorption of hydrogen (H^{*}). CHCH₂^{*} radical is subsequently hydrogenated on the catalyst surface to produce C₂H₄. The adsorbed ethylene (C₂H₄^{*}) can further hydrogenate in presence of H^{*} to generate C₂H₆ [60]. In our reaction system, the vinyl radicals may have formed directly from the adsorption of the post-plasma species-CH and CH₂ on the active metal sites followed by their hydrogenation to C₂H₄ and C₂H₆. The formation of H^{*} on Ag-Pd/CeO₂ may have been similar to that on CeO₂.

The active bimetallic (Ag-Pd) sites of the moderately heated catalyst must have redirected the post-plasma CH_x (x=0,1) radicals towards C₂ production. Since CH_x radicals are required to form HCN, the decrease in HCN selectivity was observed in this set of post-plasma reaction. The HCN concentration in the product gas mixture decreases to around 0.06% in plasma with Ag-Pd/CeO₂ reaction (Figure S-

4b). The NH_3 concentration decreased slightly from 250 ppm to around 200 ppm (Figure S-4a) which is possibly due to redirection of activated H_2 species (H , H^*) to vinyl hydrogenation. It is important to note that HCN may have been hydrogenated to NH_3 and CH_4 in presence of the heated catalyst [61,62][25] but the NH_3 concentration do not increase in the plasma reactions with Ag-Pd/CeO_2 when compared to the one with CeO_2 . Additionally, no CH_4 was observed in the product gas mixture in all the three set of plasma reactions indicating 100% conversion of methane. Hence, the reduction in HCN concentration in the product gas stream is primarily due to the redirection of CH and CH_2 radicals to C_2 products.

HCN formation is depending on the CN radical concentration in both plasma and post plasma region. The CN radical concentration in the plasma region may be reduced by optimizing the feed gas mixture such as keeping methane concentration much higher than nitrogen. This would require better cooling system, since high CH_4 feed concentration would entail high temperature (>1000 K) within the discharge region. In the post plasma region, the redirection of CH and CH_2 radicals to C_2 products decreases HCN formation, meaning more ethylene production would entail reduction in HCN selectivity. This would require designing optimum hydrogenation catalyst suitable for the post-plasma region.

Ar is known to ionize faster than other gases within the plasma region. The ionized Ar (Ar^+) may quickly transfer that charge to other reactive species such as N_2 , contributing to the formation of positively charged ions in the plasma region [63]. In low pressure plasma systems, when Ar is present in the feed gas mixture, the peaks for Ar in the OES spectra are prominent, indicative of their high degree of ionization and charge-transfer to other plasma species [51]. In our reaction system, the post-plasma region does not seem to be rich in ionized Ar species, as observed in the OES spectra (Figure 3). Hence, we can assume that Ar , even though essential in maintaining the plasma within the discharge region, does not play any major role in the post-plasma reaction.

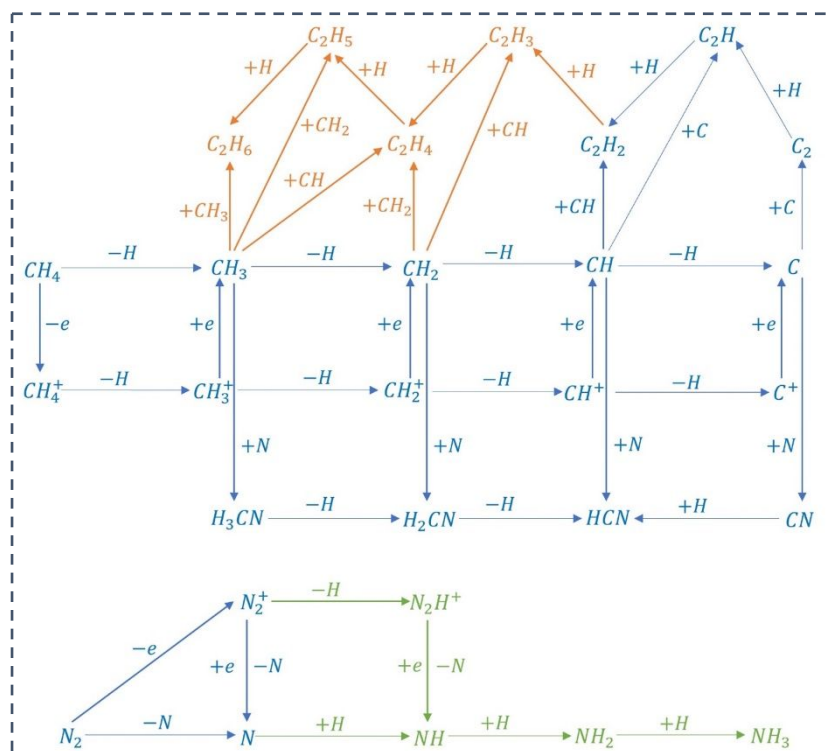


Figure 5: Hypothesized reaction mechanisms for ammonia, ethylene, HCN and ethane generation from methane and dinitrogen. Plasma reactions are shown in blue, Plasma + CeO₂: green and blue, Plasma+ Ag-Pd/CeO₂: green, blue, and orange

Based on species identified on the OES spectra and the product distribution in the three reactions, the hypothesized reaction mechanisms in the three set of reactions were summarized in Figure 5. The possible elementary reactions involved in the only plasma condition are shown in blue. The elementary reaction steps of plasma + CeO₂ are shown in green and blue and that of Ag-Pd/CeO₂ catalyst are shown in green, blue, and orange.

3.3 Influence of post-plasma species on C₂ selectivity

A catalytic reaction without plasma was conducted to further understand the significance of post-plasma species in our reaction system. As shown in Figure 2b, the Ag-Pd/CeO₂ catalyst was heated to 250°C (523 K) and fed with a gas mixture containing 1.5% H₂, 1% N₂, 0.25% C₂H₂ balanced with Ar. The content of this feed gas was similar to the product gas stream from CH₄/N₂/Ar plasma reaction. HCN could not be added to this feed gas mixture due to safety hazards. If 0.1% HCN could be added to the reaction feed mixture to exactly match the product gas mixture of plasma reaction, it may have been

hydrogenated to ammonia and methane [64]. Since no ammonia and methane were observed in the product gas mixture of this set of reaction, it can be safely assumed that if HCN was added in the feed, it would have remained unconverted during this reaction possibly due to the low reaction temperature.

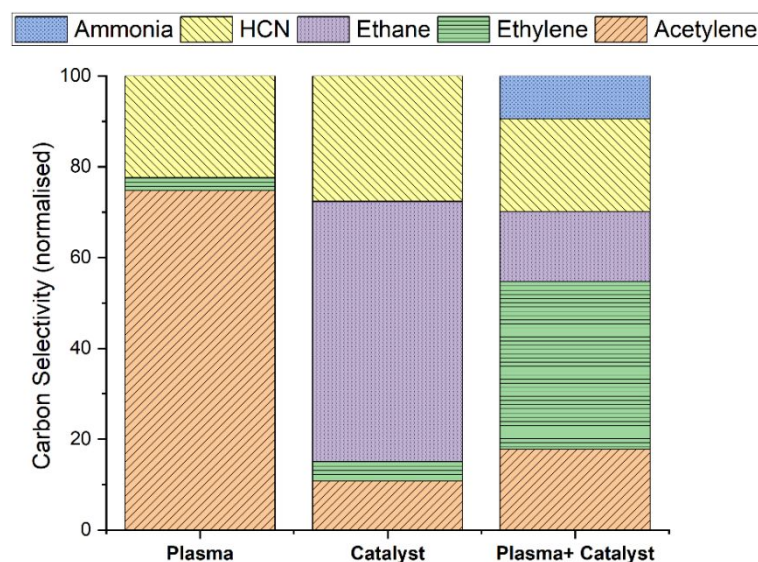


Figure 6. Normalized carbon selectivity among the C-containing products

The change in the normalized HCN and C_2 products (C_2H_2 , C_2H_4 , and C_2H_6) selectivity between three reaction scenarios: plasma, catalyst, and plasma + catalyst can be seen in Figure 6. In this figure, the plasma + Ag-Pd/Ceria reaction is designated as “plasma + catalyst.” The purpose to conduct this reaction and compare the selectivity of its C containing products to that of plasma and plasma + catalyst reaction was to demonstrate that the plasma + Ag-Pd/Ceria reaction was not merely a two-step reaction where the acetylene generated in the plasma reaction was hydrogenated to C_2 products: ethylene and ethane over the heated catalyst. As shown in Figure 6, the selectivity of acetylene was highest among the C_2 products in plasma reaction. Ethane was the dominant product in the catalytic reaction without plasma. In the plasma + catalyst reaction, the selectivity of ethylene increased considerably to around 37 %, while that of ethane reduced from 57% in catalyst reaction to 15 % in plasma + catalyst reaction. This reaction behavior was a clear indication of the post-plasma species directly influencing the C_2 product selectivity. Hence, DFT calculations were utilized to explain the interaction between the Ag-Pd/CeO₂ catalyst and the post-plasma species.

Density functional theory (DFT) calculations were performed on the hydrocarbon conversion process over the Ag-Pd (111) surface and compared with our experimental results. These DFT calculations include various adsorption configurations and the corresponding binding energies, the reaction energies, and the positively charged surface effects of acetylene, ethylene, and ethane synthesis from methane conversion. When the post-plasma species, such as $CH_x^{\delta+}$ and $NH_x^{\delta+}$, adsorb over the Ag-Pd surface, they will attract the electrons from the Ag-Pd surface and consequently, the Ag-Pd surface will become positively charged. To clarify this positive charge effect on Ag-Pd surface, XPS analysis were carried out on 1. fresh, 2. reduced and the spent Ag-Pd/CeO₂ from 3. “catalyst” and 4. “plasma + catalyst” reactions and the resultant spectra are presented in Figure 7.

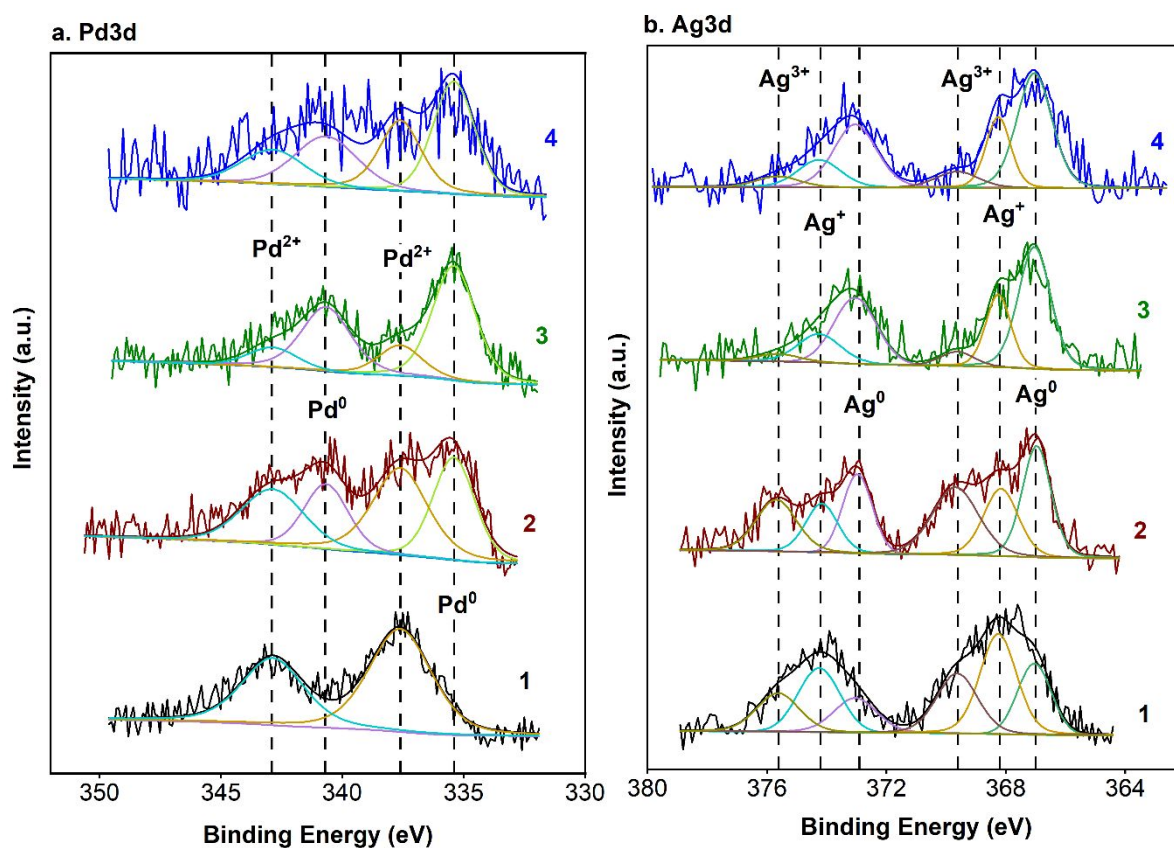


Figure 7: XPS (a) Pd3d and (b) Ag3d spectra of 1. Fresh Ag-Pd/ Ceria, 2. Reduced under 50% H₂ at 250 °C, 3. Spent Ag-Pd/ Ceria from “catalyst” reaction, 4. Spent Ag-Pd/Ceria from “plasma + catalyst” reaction

In the Gaussian deconvoluted Pd3d spectra, as shown in Figure 7a, Pd²⁺ peaks appeared at both Pd3d_{5/2} and Pd3d_{3/2} at 337.2 and 342.5 eV, respectively for the fresh Ag-Pd/CeO₂ (sample 1) [65]. The reduced catalyst (sample 2) shows splitting of the peaks into Pd²⁺ and metallic Pd⁰ at 335.6 and 341.1 eV [66].

The reduction process must have converted some of the oxidized Pd to metallic Pd on the catalyst surface. The intensities of the Pd²⁺ peaks on the Pd3d spectra of spent Ag-Pd/CeO₂ from “catalyst” reaction (sample 3) were much lower than that of sample 2, implying that sample 3 surface were mostly covered with metallic Pd. In case of the spent Ag-Pd/CeO₂ from “plasma + catalyst” reaction (sample 4), the intensities of Pd²⁺ peaks were much higher than that of sample 3, while the peak intensities of Pd⁰ slightly decreased. This was indicative of the presence of higher percentage of positively charged Pd on the catalyst surface in case of “plasma + catalyst” reaction.

In case of Ag3d spectra, as shown in Figure 7b, both Ag3d_{5/2} and Ag3d_{3/2} bands were deconvoluted into 3 peaks. The Ag3d_{5/2} had maxima at 367.9 (Ag⁰), 368.2 (Ag⁺ from Ag₂O), and 369.1 (Ag³⁺ from AgO) and Ag3d_{3/2} had maxima at 373.4 (Ag⁰), 373.9 (Ag⁺), and 375.1 (Ag³⁺)[67,68]. The intensities of these maxima varied from sample 1 to sample 4. Sample 1 was rich in Ag⁺ ions indicative of presence of Ag₂O on the catalyst surface. The treatment of the fresh catalyst with 50% hydrogen at 250°C for 1-hour partially results in the formation of metallic Ag on sample 2, where Ag⁰ had higher intensity than Ag⁺ and Ag³⁺. In case of sample 3, the intensity of Ag³⁺ reduced considerably and that of Ag⁰ peak remained the highest. Although it is hard to distinguish the spectra of sample 3 from sample 4, the intensities of the Ag⁺ species were found to be slightly higher in sample 4. This may indicate the presence of higher concentration of charged Ag on the spent catalyst surface from “plasma + catalyst” reaction.

All the samples, except the fresh catalyst, were under hydrogen rich environment at a reaction temperature of 250°C. Despite similar reaction conditions, the higher intensities of the charged Ag and Pd species on sample 4 indicate that the interaction of post plasma species with the catalyst surface leads to a positive charge effect.

To investigate the role of post-plasma species interaction with the catalyst surface on tuning the selectivity of hydrocarbons (ethylene vs. ethane), we applied DFT to calculate the C₂H₂ conversion to C₂H₄/C₂H₆. Based on the observations from four sets of experiments, including reaction occurred under plasma without any catalyst, reaction occurred over two different catalysts (CeO₂, Ag-Pd/CeO₂) at the post-plasma region (Figure 4), and reaction occurred over Ag-Pd/CeO₂ under thermal heating (Figure

6), we confirmed that the interaction between post-plasma species and Ag-Pd mainly tuned the selectivity of C_2H_2 conversion to C_2H_4/C_2H_6 .

The analysis of the XPS spectra (Figure 7) indicate the presence of Ag^+ and Pd^{2+} on the catalyst surface during the “plasma + catalyst” reaction. The oxidized state of Ag and Pd could either come from the oxygen spillover of the CeO_x support or the interaction with positively charged post-plasma species under the reaction conditions [38]. Then, we first studied the stability of the surface O^* species over the Ag-Pd from oxygen spillover in our DFT calculations via building a phase diagram (Figure S-5). Our results indicated that the O^* in the Ag-Pd surface is thermodynamically favorable to be reduced and Ag-Pd surface can be maintained in a metallic state under the experimental working conditions (250 °C, partial pressure of H_2 of 6 Pa). This result is consistent with the experimental works reported by Park et al. that Au, Cu and Pt nanoparticles remained in their metallic state even after their deposition on the reduced $CeO_x/TiO_2(110)$ surface [69]. This result is also consistent with the theoretical works reported by Aranifard et al. that the surface O^* species is not stable over the Pt cluster supported by CeO_x and Pt cluster with O^* on the surface will be reduced to metallic Pt under the experimental conditions (i.e., 100 K to 1300 K and 10^{-6} bar to 1 bar of partial pressure of H_2) [70].

After confirming the Ag-Pd model, we examined the energy diagram without plasma-species induced positively charged surface effects of CH_4 decomposition into C_1 or coupling into C_2 hydrocarbon species over Ag-Pd (Figure 8a). Our DFT results showed that, when the post-plasma species is C_2H_2 , the hydrogenation of C_2H_2 to C_2H_6 is more energetically favorable than that of C_2H_4 over the Ag-Pd surface. This explains the over-hydrogenation of acetylene to ethane in the catalyst reaction, leading to the highest ethane selectivity among the C-containing products.

Then, to investigate the role of plasma-species induced positively charged surface effects on the selectivity of C_2H_4 and C_2H_6 from methane conversion, we polarized the Ag-Pd surface to be positively charged, ranging from δ^0 to $\delta^{+0.6}$ with $\delta^{+0.1}$ increment. Interestingly, our DFT results showed that the reaction energies of the elementary steps of C_2H_4 production, including $C_2H_3 + H \leftrightarrow C_2H_4$ and $2CH_2 \leftrightarrow C_2H_4$ monotonically decreased (Figures 8b, c) as increasing the surface charges of Ag-Pd. While the

reaction energies of the elementary steps of C_2H_6 production, including $C_2H_5 + H \leftrightarrow C_2H_6$ and $2CH_3 \leftrightarrow C_2H_6$ monotonically increased (Figures 8d, e) as increasing the surface charges of Ag-Pd. This suggests that a positively charged Ag-Pd surface under the post-plasma condition, will facilitate the synthesis of C_2H_4 production than that of C_2H_6 production from CH_4 plasma. This result is consistent with previous theoretical studies reported by Bu et al. suggesting that the introduction of positive charged (100) surfaces of Pd, Au, Ag, Ni and Cu catalysts promotes acetylene adsorption and subsequently favored the production of ethylene over ethane [71]. Similarly, this result is also in agreement with the experimental works reported by Lim et al. that the application of negative electric potentials noticeably lowered the activation barriers of ethylene hydrogenation to ethane and significantly enhanced the rate of ethylene hydrogenation over Pd/C catalyst [72].

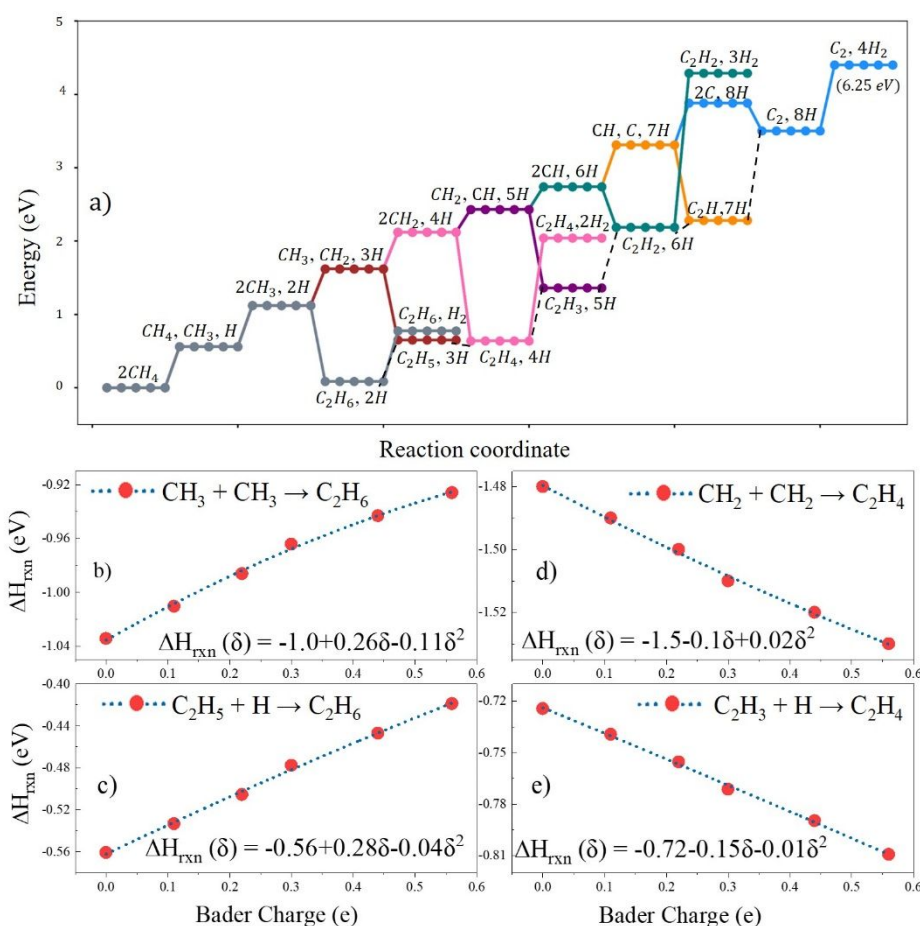


Figure 8: DFT calculations on revealing the role of positively charged surface for the C_2H_2 , C_2H_4 and C_2H_6 formation from methane conversion. (a) The energy diagram of methane decomposition into C_1 or coupling into C_2 hydrocarbon species over the Ag-Pd (111) surface. Positively charged surface effects on ethylene (b, c) and ethane (d, e) synthesis over the catalytic Ag-Pd surface.

In addition, the presence of positively charged surface significantly prevents the coke formation during methane decomposition. Our DFT energy diagram show that the energetics of carbon formation significantly increase by ~ 0.3 eV with the positive surface charges as compared to the one without charge effects (Figure S-22, Table S-2). This result is consistent with previous theoretical report from Che et al. that the positively charged Ni surface could reduce coke formation during methane steam reforming reaction [38,48,73,74]. This is also consistent with experimental work from Sekine et al., in which they stated that the introduction of positive voltage removed the formation of reactive carbon (such as C_α and C_β) deposition during toluene steam reforming, and significantly suppressed coke formation during the process [75]. Yet et al. also reported that external positive applied potential reduces the surface coverage of carbon and accelerates the rate-determining step of the $C - H$ bond cleavage in methane over IrO_2 [76]. The linear relationship between the activation barrier and the reaction energy of hydrocarbon-related elementary reactions over different transition metal surfaces, known as the *Brønsted – Evans – Polanyi (BEP)* relation, has been determined by many researchers from DFT calculations [77] [78][79] [80] [81] [82] [83] [84] [85]. Che et al. also proved that the BEP relation for the C-H bond cleavage is still validated when different surface charges were applied via adding external electric fields [48]. Such BEP relation could be employed this current work to estimate the kinetic behavior (i.e., activation barriers) of C-H bond cleavage and C-C bond formation based on our calculated thermodynamics properties (i.e., reaction energy in Figure 8). Therefore, the conclusion derived from thermodynamic properties will hold for the kinetic parameters. In our experiments, the breakdown of methane begins within the MW cavity where the plasma is generated. The CH_x ($x=0,1,2,3$) radicals, hence formed, travel down to the heated catalyst bed. As per the DFT results, these radicals will be less likely to form coke at atmospheric pressure and moderate temperature of 250 °C.

Conclusion

This article has successfully demonstrated the charge effects of post-plasma species and moderately heated catalyst in improving the selectivity of ethylene over ethane while reducing unwanted by-product such as HCN. DFT calculations were used to determine the post-plasma induced positive charge effects

on the catalytic Ag-Pd surface during the post-plasma reaction, leading to better ethylene selectivity and reducing its over-hydrogenation to ethane.

To decarbonize the chemical industry, a significant amount of effort is being directed towards non-oxidative and direct utilization of CH₄. Since natural gas is indeed an important raw material for chemicals, its efficient utilization can significantly reduce the carbon footprint of chemical industries. Microwave enhanced-plasma assisted methane conversion [12] and ammonia synthesis [86] has the potential to become modular-scale green alternative to large-scale commercial processes. Despite offering several advantages such as fast process dynamics and flexibility, high selectivity towards desired products, and reducing unwanted by-products, the commercialization of plasma based chemical processing remains a challenge to present day.

The major bottleneck is the input energy requirement to match the throughput of current industries [5]. To address this scaling issue, it is advisable to build modular systems at the source of the raw material that can be run on intermittent-renewable energy sources and be tuned as per the market demand and power availability. Furthermore, integrating highly-efficient catalytic material into the plasma reactor can contribute to overall energy-efficiency. The current research pertaining to plasma-catalysis, specifically non-thermal plasma, have been focused on optimizing energy requirements, conversion, and selectivity [87]. There is also an increasing trend in studies that investigate the underlying mechanism behind plasma-catalyst synergy using simulations and in-situ analysis [13]. The proof-of-experiment presented in this paper demonstrated the conversion of methane to two very important end-products, NH₃ and C₂H₄ without CO₂ emissions. Such a reactor could be utilized as small-scale modular processing units that can operate with renewable energy at the production stage of natural gas, eliminating the bottlenecks associated with transportation. By utilizing DFT calculations, this article showed that a better selectivity towards ethylene can be achieved by the charge-effect induced by post-plasma species on the catalytic surface. Hence establishing a possible reaction mechanism leading to better product selectivity.

Further understanding the underlying mechanism behind plasma and catalyst interaction would help optimize the reaction and catalyst design, leading to the development of reaction kinetic models.

Designing reactors with low energy and material cost, stability and longevity would lower the overall production cost. Overcoming these scientific and engineering challenges is instrumental to wider industrial application of plasma catalysis in methane utilization.

Acknowledgements

The authors acknowledge financial support from the West Virginia Higher Education Policy Commission under Grant HEPC.dsr.18.7. F. Che and S. AhmatIbrahim were partially supported by institutional faculty start-up funds from University of Massachusetts Lowell and partially sponsored by the Department of the Navy, Office of Naval Research award No. 1172044/2/93083. F. Che and S. AhmatIbrahim also acknowledge the computational resources provided by Massachusetts Green High Performance Computing Center (MGHPCC) and Center for Nanophase Materials Sciences at Oak Ridge National Lab through CNMS2021-A-00602 proposal award.

References

- [1] Shale Gas and Other Unconventional Sources of Natural Gas | Union of Concerned Scientists, (2015). <https://www.ucsusa.org/resources/shale-gas-and-other-sources-natural-gas#references>.
- [2] S. Sitter, Q. Chen, I.E. Grossmann, An overview of process intensification methods, *Curr Opin Chem Eng.* 25 (2019) 87–94. <https://doi.org/10.1016/J.COCH.2018.12.006>.
- [3] Peter Levi, Tiffany Vass, Hana Mandová, Alexandre Gouy, *Chemicals – Tracking Report (IEA)*, 2020. <https://www.iea.org/reports/chemicals>.
- [4] T. Van Gerven, A. Stankiewicz, Structure, energy, synergy, time—the fundamentals of process intensification, *Ind Eng Chem Res.* 48 (2009) 2465–2474. <https://doi.org/10.1021/ie801501y>.
- [5] J.F. de la. Fuente, A.A. Kiss, M.T. Radoiu, G.D. Stefanidis, Microwave plasma emerging technologies for chemical processes, *Journal of Chemical Technology and Biotechnology.* 92 (2017) 2495–2505. <https://doi.org/10.1002/jctb.5205>.
- [6] S. Tiwari, A. Caiola, X. Bai, A. Lalsare, J. Hu, Microwave Plasma-Enhanced and Microwave Heated Chemical Reactions, *Plasma Chemistry and Plasma Processing.* 40 (2020) 1–23. <https://doi.org/10.1007/s11090-019-10040-7>.
- [7] C.M. Ferreira, M. Moisan, *Microwave discharges: fundamentals and applications*, Springer Science & Business Media, 2013.
- [8] C. Shen, Y. Sun, D. Sun, H. Yang, A study on methane coupling to acetylene under the microwave plasma, *Sci China Chem.* 53 (2010) 231–237. <https://doi.org/10.1007/s11426-010-0016-0>.

- [9] C. Shen, D. Sun, H. Yang, Methane coupling in microwave plasma under atmospheric pressure, *Journal of Natural Gas Chemistry*. 20 (2011) 449–456. [https://doi.org/10.1016/S1003-9953\(10\)60209-5](https://doi.org/10.1016/S1003-9953(10)60209-5).
- [10] M. Heintze, M. Magureanu, Methane conversion into acetylene in a microwave plasma: Optimization of the operating parameters, *J Appl Phys*. 92 (2002) 2276–2283. <https://doi.org/10.1063/1.1497457>.
- [11] M. Wnukowski, A.W. van de Steeg, B. Hrycak, M. Jasiński, G.J. van Rooij, Influence of hydrogen addition on methane coupling in a moderate pressure microwave plasma, *Fuel*. 288 (2021). <https://doi.org/10.1016/j.fuel.2020.119674>.
- [12] M. Scapinello, E. Delikonstantis, G.D. Stefanidis, The panorama of plasma-assisted non-oxidative methane reforming, *Chemical Engineering and Processing: Process Intensification*. 117 (2017) 120–140. <https://doi.org/10.1016/J.CEP.2017.03.024>.
- [13] A. Bogaerts, X. Tu, J.C. Whitehead, G. Centi, L. Lefferts, O. Guaitella, F. Azzolina-Jury, H.H. Kim, A.B. Murphy, W.F. Schneider, T. Nozaki, J.C. Hicks, A. Rousseau, F. Thevenet, A. Khacef, M. Carreon, The 2020 plasma catalysis roadmap, *J Phys D Appl Phys*. 53 (2020). <https://doi.org/10.1088/1361-6463/ab9048>.
- [14] J.L. Jauberteau, I. Jauberteau, Synthesis of cyanides in N₂-CH₄ discharge afterglow, *J Phys D Appl Phys*. 51 (2018). <https://doi.org/10.1088/1361-6463/aacc2>.
- [15] A.M. Diamy, R. Hrach, V. Hrachová, J.C. Legrand, Influence of C atom concentration for acetylene production in a CH₄/N₂ afterglow, *Vacuum*. 61 (2001) 403–407. [https://doi.org/10.1016/S0042-207X\(01\)00151-8](https://doi.org/10.1016/S0042-207X(01)00151-8).
- [16] J.L. Jauberteau, L. Thomas, J. Aubreton, I. Jauberteau, A. Catherinot, High reactivity of CH₂ radical in an AR-CH₄ post-discharge, *Plasma Chemistry and Plasma Processing*. 18 (1998) 137–151. <https://doi.org/10.1023/A:1021797428416>.
- [17] C.L. Gordon, L.L. Lobban, R.G. Mallinson, Ethylene production using a Pd and Ag–Pd–Y-zeolite catalyst in a DC plasma reactor, *Catal Today*. 84 (2003) 51–57. [https://doi.org/10.1016/S0920-5861\(03\)00300-6](https://doi.org/10.1016/S0920-5861(03)00300-6).
- [18] S. Kado, Y. Sekine, K. Urasaki, K. Okazaki, T. Nozaki, High performance methane conversion into valuable products with spark discharge at room temperature, *Stud Surf Sci Catal*. 147 (2004) 577–582. [https://doi.org/10.1016/S0167-2991\(04\)80114-9](https://doi.org/10.1016/S0167-2991(04)80114-9).
- [19] K. Wang, X. Li, A. Zhu, A Green Process for High-Concentration Ethylene and Hydrogen Production from Methane in a Plasma-Followed-by-Catalyst Reactor, *Plasma Science and Technology*. 13 (2011) 77. <https://doi.org/10.1088/1009-0630/13/1/16>.
- [20] B. Wang, H.M. Guan, Highly Efficient Conversion of Methane to Olefins via a Recycle-Plasma-Catalyst Reactor, *Catal Letters*. 146 (2016) 2193–2199. <https://doi.org/10.1007/S10562-016-1846-Y/FIGURES/8>.
- [21] E. Delikonstantis, M. Scapinello, G.D. Stefanidis, Low energy cost conversion of methane to ethylene in a hybrid plasma-catalytic reactor system, *Fuel Processing Technology*. 176 (2018) 33–42. <https://doi.org/10.1016/J.FUPROC.2018.03.011>.

- [22] E.C. Neyts, K. Ostrikov, M.K. Sunkara, A. Bogaerts, Plasma Catalysis: Synergistic Effects at the Nanoscale, *Chem Rev.* 115 (2015) 13408–13446. <https://doi.org/10.1021/acs.chemrev.5b00362>.
- [23] H.H. Kim, Y. Teramoto, A. Ogata, H. Takagi, T. Nanba, Plasma Catalysis for Environmental Treatment and Energy Applications, *Plasma Chemistry and Plasma Processing.* 36 (2016) 45–72. <https://doi.org/10.1007/s11090-015-9652-7>.
- [24] S. Xu, S. Chansai, C. Stere, B. Inceesungvorn, A. Goguet, K. Wangkawong, S.F.R. Taylor, N. Al-Janabi, C. Hardacre, P.A. Martin, X. Fan, Sustaining metal–organic frameworks for water–gas shift catalysis by non-thermal plasma, *Nat Catal.* 2 (2019) 142–148. <https://doi.org/10.1038/s41929-018-0206-2>.
- [25] Y. Yi, X. Wang, A. Jafarzadeh, L. Wang, P. Liu, B. He, J. Yan, R. Zhang, H. Zhang, X. Liu, H. Guo, E.C. Neyts, A. Bogaerts, Plasma-Catalytic Ammonia Reforming of Methane over Cu-Based Catalysts for the Production of HCN and H₂ at Reduced Temperature, *ACS Catal.* 11 (2021) 1765–1773. <https://doi.org/10.1021/acscatal.0c04940>.
- [26] M. Heintze, M. Magureanu, M. Kettlitz, Mechanism of C₂ hydrocarbon formation from methane in a pulsed microwave plasma, *J Appl Phys.* 92 (2002) 7022–7031. <https://doi.org/10.1063/1.1521518>.
- [27] D. Teschner, E. Vass, M. Hävecker, S. Zafeirotos, P. Schnörch, H. Sauer, A. Knop-Gericke, R. Schlögl, M. Chamam, A. Wootsch, A.S. Canning, J.J. Gamman, S.D. Jackson, J. McGregor, L.F. Gladden, Alkyne hydrogenation over Pd catalysts: A new paradigm, *J Catal.* 242 (2006) 26–37. <https://doi.org/10.1016/J.JCAT.2006.05.030>.
- [28] A.J. McCue, J.A. Anderson, Recent advances in selective acetylene hydrogenation using palladium containing catalyst, *Front Chem Sci Eng.* 9 (2015) 142–153. <https://doi.org/10.1007/s11705-015-1516-4>.
- [29] F. Zaera, The Surface Chemistry of Metal-Based Hydrogenation Catalysis, *ACS Catal.* 7 (2017) 4947–4967. <https://doi.org/10.1021/acscatal.7b01368>.
- [30] N.A. Khan, S. Shaikhutdinov, H.J. Freund, Acetylene and ethylene hydrogenation on alumina supported Pd-Ag model catalysts, *Catal Letters.* 108 (2006) 159–164. <https://doi.org/10.1007/s10562-006-0041-y>.
- [31] H. Zea, K. Lester, A.K. Datye, E. Rightor, R. Gulotty, W. Waterman, M. Smith, The influence of Pd–Ag catalyst restructuring on the activation energy for ethylene hydrogenation in ethylene–acetylene mixtures, *Appl Catal A Gen.* 282 (2005) 237–245. <https://doi.org/10.1016/J.APCATA.2004.12.026>.
- [32] Y. Zhang, W. Diao, C.T. Williams, J.R. Monnier, Selective hydrogenation of acetylene in excess ethylene using Ag- and Au–Pd/SiO₂ bimetallic catalysts prepared by electroless deposition, *Appl Catal A Gen.* 469 (2014) 419–426. <https://doi.org/10.1016/J.APCATA.2013.10.024>.
- [33] W. Huang, W. Pyrz, R.F. Lobo, J.G. Chen, Selective hydrogenation of acetylene in the presence of ethylene on K⁺-β-zeolite supported Pd and PdAg catalysts, *Appl Catal A Gen.* 333 (2007) 254–263. <https://doi.org/10.1016/J.APCATA.2007.09.017>.
- [34] S. Zhang, C.-R. Chang, Z.-Q. Huang, J. Li, Z. Wu, Y. Ma, Z. Zhang, Y. Wang, Y. Qu, High Catalytic Activity and Chemoselectivity of Sub-nanometric Pd Clusters on Porous Nanorods of CeO₂ for

- Hydrogenation of Nitroarenes, *J Am Chem Soc.* 138 (2016) 2629–2637.
<https://doi.org/10.1021/jacs.5b11413>.
- [35] S. Zhang, J. Li, Z. Xia, C. Wu, Z. Zhang, Y. Ma, Y. Qu, Towards highly active Pd/CeO₂ for alkene hydrogenation by tuning Pd dispersion and surface properties of the catalysts, *Nanoscale.* 9 (2017) 3140–3149. <https://doi.org/10.1039/C6NR09297G>.
- [36] Y. Zhang, C. Chen, W. Gong, J. Song, H. Zhang, Y. Zhang, G. Wang, H. Zhao, Self-assembled Pd/CeO₂ catalysts by a facile redox approach for high-efficiency hydrogenation of levulinic acid into gamma-valerolactone, *Catal Commun.* 93 (2017) 10–14.
<https://doi.org/10.1016/J.CATCOM.2017.01.008>.
- [37] S. Tiwari, A. Caiola, X. Bai, A. Lalsare, J. Hu, Microwave Plasma-Enhanced and Microwave Heated Chemical Reactions, *Plasma Chemistry and Plasma Processing.* 40 (2020) 1–23.
<https://doi.org/10.1007/S11090-019-10040-7/METRICS>.
- [38] F. Che, J.T. Gray, S. Ha, N. Kruse, S.L. Scott, J.-S. McEwen, Elucidating the Roles of Electric Fields in Catalysis: A Perspective, *ACS Catal.* 8 (2018) 5153–5174.
<https://doi.org/10.1021/acscatal.7b02899>.
- [39] F. Che, R. Zhang, J.A. Hensley, S. Ha, J.-S. McEwen, Density functional theory studies of methyl dissociation on a Ni (111) surface in the presence of an external electric field, *Physical Chemistry Chemical Physics.* 16 (2014) 2399–2410.
<https://doi.org/https://doi.org/10.1039/C3CP54135E>.
- [40] J.P. Perdew, K. Burke, M. Ernzerhof, Generalized gradient approximation made simple, *Phys Rev Lett.* 77 (1996) 3865–3868. <https://doi.org/10.1103/PHYSREVLETT.77.3865>.
- [41] G. Kresse, J. Furthmüller, Efficient iterative schemes for ab initio total-energy calculations using a plane-wave basis set, *Phys Rev B.* 54 (1996) 11 169–11 186.
<https://doi.org/https://doi.org/10.1103/PhysRevB.54.11169>.
- [42] G. Kresse, J. Hafner, Norm-conserving and ultrasoft pseudopotentials for first-row and transition elements, *Phys Rev B.* 6 (1994) 8245. <https://doi.org/10.1088/0953-8984/6/40/015>.
- [43] M. Wan, H. Yue, J. Notarangelo, H. Liu, F. Che, Deep Learning-Assisted Investigation of Electric Field–Dipole Effects on Catalytic Ammonia Synthesis, *JACS Au.* (2022).
<https://doi.org/10.1021/JACSAU.2C00003>.
- [44] S.M. Foiles, M.I. Baskes, M.S. Daw, Embedded-atom-method functions for the fcc metals Cu, Ag, Au, Ni, Pd, Pt, and their alloys, *Phys Rev B.* 33 (1986) 7983–7991.
<https://doi.org/10.1103/PHYSREVB.33.7983>.
- [45] D.S. Su, T. Jacob, T.W. Hansen, D. Wang, R. Schlögl, B. Freitag, S. Kujawa, Surface Chemistry of Ag Particles: Identification of Oxide Species by Aberration-Corrected TEM and by DFT Calculations, *Angewandte Chemie.* 120 (2008) 5083–5086.
<https://doi.org/10.1002/ANGE.200800406>.
- [46] E. Jette, F.F.-T.J. of C. Physics, undefined 1935, Precision determination of lattice constants, *Aip.Scitation.Org.* 3 (1935) 605–616. <https://doi.org/10.1063/1.1749562>.
- [47] B.N. Dutta, B. Dayal, Lattice Constants and Thermal Expansion of Palladium and Tungsten up to 878 °C by X-Ray Method, *Physica Status Solidi (b).* 3 (1963) 2253–2259.
<https://doi.org/10.1002/PSSB.19630031207>.

- [48] F. Che, J.T. Gray, S. Ha, J.S. McEwen, Improving Ni Catalysts Using Electric Fields: A DFT and Experimental Study of the Methane Steam Reforming Reaction, *ACS Catal.* 7 (2017) 551–562. <https://doi.org/10.1021/ACSCATAL.6B02318>.
- [49] P. Deshlahra, E.E. Wolf, W.F. Schneider, A periodic density functional theory analysis of CO chemisorption on Pt (111) in the presence of uniform electric fields, *Journal of Physical Chemistry A.* 113 (2009) 4125–4133. <https://doi.org/10.1021/jp810518x>.
- [50] P. Kouakou, V. Brien, B. Assouar, V. Hody, M. Belmahi, H.N. Migeon, J. Bougdira, Preliminary synthesis of carbon nitride thin films by N₂/CH₄ microwave plasma assisted chemical vapour deposition: Characterisation of the discharge and the obtained films, *Plasma Processes and Polymers.* 4 (2007) 210–214. <https://doi.org/10.1002/ppap.200730703>.
- [51] L. Salazar-Flores, C. Torres-Segundo, P.G. Reyes, F. Castillo, H. Martinez, Low-pressure plasma discharge of Ar/N₂/CH₄ ternary mixture: Experimental simulation of Titan's atmosphere, *J Phys Conf Ser.* 511 (2014) 0–4. <https://doi.org/10.1088/1742-6596/511/1/012055>.
- [52] G. Horvath, F. Krcma, L. Polachova, K. Klohnova, N.J. Mason, M. Zahoran, S. Matejcik, Organic chemistry of NH₃ and HCN induced by an atmospheric abnormal glow discharge in N₂-CH₄ mixtures, *EPJ Applied Physics.* 53 (2011). <https://doi.org/10.1051/epjap/2010100191>.
- [53] T.L. Van Surksun, E.R. Fisher, Elucidating energetics and kinetics in environmentally relevant mixed gas plasmas.pdf, *Journal of Vacuum Science & Technology A: Vacuum, Surfaces, and Films.* 39 (2021) 1–15. <https://doi.org/10.1116/6.0001080>.
- [54] M. Bai, Z. Zhang, M. Bai, X. Bai, H. Gao, Synthesis of Ammonia using CH₄/N₂ plasmas based on micro-gap discharge under environmentally friendly condition, *Plasma Chemistry and Plasma Processing.* 28 (2008) 405–414. <https://doi.org/10.1007/s11090-008-9132-4>.
- [55] C. Szopa, G. Cernogora, L. Boufendi, J.J. Correia, P. Coll, PAMPRE: A dusty plasma experiment for Titan's tholins production and study, *Planet Space Sci.* 54 (2006) 394–404. <https://doi.org/10.1016/J.PSS.2005.12.012>.
- [56] G. Horvath, J.D. Skalny, N.J. Mason, M. Klas, M. Zahoran, R. Vladioiu, M. Manole, Corona discharge experiments in admixtures of N₂ and CH₄: A laboratory simulation of Titan's atmosphere, *Plasma Sources Sci Technol.* 18 (2009) 0–7. <https://doi.org/10.1088/0963-0252/18/3/034016>.
- [57] G. Dilecce, P.F. Ambrico, G. Scarduelli, P. Tosi, S. De Benedictis, CN(B₂σ⁺) formation and emission in a N₂-CH₄ atmospheric pressure dielectric barrier discharge, *Plasma Sources Sci Technol.* 18 (2009). <https://doi.org/10.1088/0963-0252/18/1/015010>.
- [58] M. Bai, Z. Zhang, M. Bai, X. Bai, H. Gao, Synthesis of Ammonia Using CH₄/N₂ Plasmas Based on Micro-Gap Discharge under Environmentally Friendly Condition, *Plasma Chemistry and Plasma Processing* 2008 28:4. 28 (2008) 405–414. <https://doi.org/10.1007/S11090-008-9132-4>.
- [59] L. Torokova, J. Watson, F. Krcma, V. Mazankova, N.J. Mason, G. Horvath, S. Matejcik, Gas Chromatography Analysis of Discharge Products in N₂-CH₄ Gas Mixture at Atmospheric Pressure: Study of Mimic Titan's Atmosphere, *Contributions to Plasma Physics.* 55 (2015) 470–480. <https://doi.org/10.1002/ctpp.201400052>.

- [60] D. Mei, M. Neurock, C.M. Smith, Hydrogenation of acetylene-ethylene mixtures over Pd and Pd-Ag alloys: First-principles-based kinetic Monte Carlo simulations, *J Catal.* 268 (2009) 181–195. <https://doi.org/10.1016/j.jcat.2009.09.004>.
- [61] M.K. Hsiao, W.T. Lo, J.H. Wang, H.L. Chen, Hydrogenation of Hydrogen Cyanide to Methane and Ammonia by a Metal Catalyst: Insight from First-Principles Calculations, *Journal of Physical Chemistry C.* 120 (2016) 22946–22956. <https://doi.org/10.1021/acs.jpcc.6b06490>.
- [62] F. Wang, Y. Lv, W. Xueqian, Y. Ma, P. Ning, Hydrogen cyanide removal over Ti-Al₂O₃ Catalyst: Activity at low temperature, *Environ Eng Sci.* 36 (2019) 1011–1018. <https://doi.org/10.1089/ees.2018.0562>.
- [63] J. Nakajima, H. Sekiguchi, Synthesis of ammonia using microwave discharge at atmospheric pressure, *Thin Solid Films.* 516 (2008) 4446–4451. <https://doi.org/10.1016/J.TSF.2007.10.053>.
- [64] M.-K. Hsiao, W.-T. Lo, J.-H. Wang, H.-L. Chen, Hydrogenation of Hydrogen Cyanide to Methane and Ammonia by a Metal Catalyst: Insight from First-Principles Calculations, *Journal of Physical Chemistry C.* 120 (2016) 22946–22956. <https://doi.org/10.1021/acs.jpcc.6b06490>.
- [65] M.C. Militello, S.J. Simko, Palladium Oxide (PdO) by XPS, *Surface Science Spectra.* 3 (2021) 395. <https://doi.org/10.1116/1.1247784>.
- [66] R.T. Poole, P.C. Kemeny, J. Liesegang, J.G. Jenkin, R.C.G. Leckey, High resolution photoelectron studies of the d bands of some metals, *Journal of Physics F: Metal Physics.* 3 (1973) L46. <https://doi.org/10.1088/0305-4608/3/3/005>.
- [67] Y. Xu, H. You, TiO₂ modified with Ag nanoparticles synthesized via ultrasonic atomization-UV reduction and the use of kinetic models to determine the acetic acid photocatalytic degradation, *Appl Surf Sci.* 321 (2014) 481–487. <https://www.sciencedirect.com/science/article/pii/S0169433214022338> (accessed February 28, 2023).
- [68] L.M. Santos, W.A. Machado, M.D. França, K.A. Borges, R.M. Paniago, A.O.T. Patrocinio, A.E.H. Machado, Structural characterization of Ag-doped TiO₂ with enhanced photocatalytic activity, *RSC Adv.* 5 (2015) 103752–103759. <https://doi.org/10.1039/C5RA22647C>.
- [69] J.B. Park, J. Graciani, J. Evans, D. Stacchiola, S.D. Senanayake, L. Barrio, P. Liu, J.F. Sanz, J. Hrbek, J.A. Rodriguez, Gold, copper, and platinum nanoparticles dispersed on CeO_x/TiO₂(110) surfaces: High water-gas shift activity and the nature of the mixed-metal oxide at the nanometer level, *J Am Chem Soc.* 132 (2010) 356–363. <https://doi.org/10.1021/JA9087677>.
- [70] S. Aranifard, S. Ammal, A.H.-T.J. of Physical, undefined 2012, Nature of Ptn/CeO₂ (111) Surface under Water–Gas Shift Reaction Conditions: A Constrained ab Initio Thermodynamics Study, ACS Publications. (n.d.). <https://pubs.acs.org/doi/abs/10.1021/jp300515b> (accessed February 11, 2023).
- [71] J. Bu, Z. Liu, W. Ma, L. Zhang, T. Wang, H. Zhang, Q. Zhang, X. Feng, J. Zhang, Selective electrocatalytic semihydrogenation of acetylene impurities for the production of polymer-grade ethylene, *Nat Catal.* 4 (2021) 557–564. <https://doi.org/10.1038/s41929-021-00641-x>.
- [72] C.W. Lim, M.J. Hülsey, N. Yan, Non-Faradaic Promotion of Ethylene Hydrogenation under Oscillating Potentials, *JACS Au.* 1 (2021) 536–542. <https://doi.org/10.1021/JACSAU.1C00044>.

- [73] F. Che, R. Zhang, J.A. Hensley, S. Ha, J.-S. McEwen, Density functional theory studies of methyl dissociation on a Ni (111) surface in the presence of an external electric field, *Physical Chemistry Chemical Physics*. 16 (2014) 2399–2410. <https://doi.org/10.1039/C3CP54135E>.
- [74] F. Che, S. Ha, J.-S. McEwen, Elucidating the field influence on the energetics of the methane steam reforming reaction: A density functional theory study, *Appl Catal B*. 195 (2016) 77–89. <https://doi.org/https://doi.org/10.1016/j.apcatb.2016.04.026>.
- [75] K. Takise, A. Sato, K. Muraguchi, S. Ogo, Y. Sekine, Steam reforming of aromatic hydrocarbon at low temperature in electric field, *Appl Catal A Gen*. 573 (2019) 56–63. <https://doi.org/https://doi.org/10.1016/j.apcata.2019.01.011>.
- [76] C.-H. Yeh, T.M. le Pham, S. Nachimuthu, J.-C. Jiang, Effect of External Electric Field on Methane Conversion on IrO₂(110) Surface: A Density Functional Theory Study, *ACS Catal*. 9 (2019) 8230–8242. <https://doi.org/10.1021/acscatal.9b01910>.
- [77] A. Logadottir, T.H. Rod, J.K. Nørskov, B. Hammer, S. Dahl, C.J.H. Jacobsen, The Brønsted-Evans-Polanyi relation and the volcano plot for ammonia synthesis over transition metal catalysts, *J Catal*. 197 (2001) 229–231. <https://doi.org/10.1006/jcat.2000.3087>.
- [78] A. Vojvodic, F. Calle-Vallejo, W. Guo, S. Wang, A. Toftelund, F. Studt, J.I. Martínez, J. Shen, I.C. Man, J. Rossmeisl, T. Bligaard, J.K. Nørskov, F. Abild-Pedersen, On the behavior of Brønsted-Evans-Polanyi relations for transition metal oxides, *J Chem Phys*. 134 (2011) 244509. <https://doi.org/10.1063/1.3602323>.
- [79] D. Loffreda, F. Delbecq, F. Vigné, P. Sautet, Fast Prediction of Selectivity in Heterogeneous Catalysis from Extended Brønsted–Evans–Polanyi Relations: A Theoretical Insight, *Angewandte Chemie*. 121 (2009) 9140–9142. <https://doi.org/10.1002/ANGE.200902800>.
- [80] F. Viñes, A. Vojvodic, F. Abild-Pedersen, F. Illas, Brønsted-Evans-Polanyi Relationship for Transition Metal Carbide and Transition Metal Oxide Surfaces, *Journal of Physical Chemistry C*. 117 (2013) 4168–4171. <https://doi.org/10.1021/JP312671Z>.
- [81] T. Bligaard, J. Nørskov, S. Dahl, J. Matthiesen, C.H. Christensen, J. Sehested, The Brønsted–Evans–Polanyi relation and the volcano curve in heterogeneous catalysis, *J Catal*. 224 (2004) 216–217. <https://doi.org/https://doi.org/10.1016/j.jcat.2004.02.034>.
- [82] V. Pallassana, M. Neurock, Electronic factors governing ethylene hydrogenation and dehydrogenation activity of pseudomorphic PdML/Re (0001), PdML/Ru (0001), Pd (111), and PdML/Au (111), *J Catal*. 191 (2000) 301–317. <https://www.sciencedirect.com/science/article/abs/pii/S0021951799927240> (accessed November 8, 2022).
- [83] R.S. Assary, L.J. Broadbelt, L.A. Curtiss, Brønsted-Evans-Polanyi relationships for C-C bond forming and C-C bond breaking reactions in thiamine-catalyzed decarboxylation of 2-keto acids using density functional theory, *J Mol Model*. 18 (2012) 145–150. <https://doi.org/10.1007/S00894-011-1062-Z>.
- [84] J.L.C. Fajín, F. Viñes, M.N.D.S. Cordeiro, F. Illas, J.R.B. Gomes, Effect of the Exchange-Correlation Potential on the Transferability of Brønsted-Evans-Polanyi Relationships in Heterogeneous Catalysis, *J Chem Theory Comput*. 12 (2016) 2121–2126. <https://doi.org/10.1021/ACS.JCTC.6B00168>.

- [85] J. Cheng, P. Hu, P. Ellis, S. French, G. Kelly, C.M. Lok, Brønsted-Evans-Polanyi relation of multistep reactions and volcano curve in heterogeneous catalysis, *Journal of Physical Chemistry C*. 112 (2008) 1308–1311. <https://doi.org/10.1021/JP711191J>.
- [86] J. Hong, S. Praver, A.B. Murphy, Plasma Catalysis as an Alternative Route for Ammonia Production: Status, Mechanisms, and Prospects for Progress, *ACS Sustain Chem Eng*. 6 (2018) 15–31. <https://doi.org/10.1021/acssuschemeng.7b02381>.
- [87] V. Hessel, G. Cravotto, P. Fitzpatrick, B.S. Patil, J. Lang, W. Bonrath, Industrial applications of plasma, microwave and ultrasound techniques: Nitrogen-fixation and hydrogenation reactions, *Chemical Engineering and Processing: Process Intensification* . 71 (2013) 19–30. <https://www.sciencedirect.com/science/article/pii/S0255270113000391> (accessed February 14, 2023).